Rheological Characteristics of Molten Salt Seeded with Al₂O₃ Nanopowder and Graphene for Concentrated Solar Power

Xin Xiao [1,*], **Gan Zhang** [2], **Yulong Ding** [2] and **Dongsheng Wen** [1,3,*]

1   School of Chemical and Process Engineering, University of Leeds, Leeds LS2 9JT, UK
2   Birmingham Centre for Energy Storage, School of Chemical Engineering, University of Birmingham, Birmingham B15 2TT, UK; willzhangdegan@hotmail.com (G.Z.); y.ding@bham.ac.uk (Y.D.)
3   School of Aeronautic Science and Engineering, Beihang University, Beijing 100191, China
*   Correspondence: x.xiao@leeds.ac.uk or xiaoxwe83@163.com (X.X.); d.wen@leeds.ac.uk (D.W.);
    Tel.: +44 (0)113-343-1299 (X.X.)

Abstract: HITEC salt (NaNO₂-NaO₃-KNO₃) and solar salt (NaO₃-KNO₃) are typical molten salts used in concentrated solar power. Adding nanoparticles is an effective method to improve the thermo-physical properties of pure salt. It is indispensable to experimentally study the rheological behaviours of salt seeded with nanoparticles, which can increase the specific heat capacity of pure salt. In this work, the viscosities of HITEC salt were measured with different shear rates in the temperature range of 200 °C to 450 °C firstly, while those of solar salt were measured in the temperature range of 250 °C to 500 °C. The experimental data showed reasonable agreement with the literature correlations, which verify the Newtonian behaviours of pure salts. The evolutions of the viscosities of nanocomposites in the same temperature range were measured and analysed, where the nanocomposites were synthesized with 1 wt.% or 2 wt.% Al₂O₃ nanopowder and graphene, respectively. Results showed that the addition of Al₂O₃ nanopowder had relatively little effect on viscosity, and the variations were about −35.4%~8.1% for the HITEC salt nanocomposites and −9.2%~68.1% for the solar salt nanocomposites. While graphene would apparently increase the viscosities of HITEC salt and solar salt, HITEC salt with the addition of graphene showed slight non-Newtonian fluid behaviour.

Keywords: molten salt; aluminium oxide nanopowder; graphene; rheological behaviour

1. Introduction

Nowadays fossil fuel energy resources are severely reduced, which is causing an increasing demand for the development and application of suitable alternative energies, especially solar energy, which is a renewable energy [1]. Concentrated solar thermal power (CSP) is one of the main technologies for solar energy utilization [2–5], while the suitability of a solar collector should be chosen according to the testing conditions specified in the existing standards [6]. A CSP system always uses heat transfer fluid (HTF) to send the intense heat to a thermal power plant which is able to provide power at night-time with the amount of stored thermal energy. Thus, a CSP system combined with a thermal energy storage system becomes the first choice to provide flexible and consistent power [7,8]. The development of reliable thermal storage system is vital for the sustainable and efficient utilization of solar energy resource.

Because of their large specific heat capacity, low viscosity, wide temperature range, and good compatibility with containers, molten salts have been widely used as latent thermal storage media in solar power fields [9,10]. Molten salts are also used as HTFs to store sensible heat, and they are

considered as an alternative to oils because of their low cost and harmlessness to the environment [11]. There are many studies conducted about molten salts, including their thermo-physical properties and system performances [12–14]. Siegel et al. [13] measured the thermo-physical properties of several molten salt mixtures, such as ternary eutectic salt (Na-K-Li, Na-K-Ca), quaternary eutectic salt (Na-K-Li-Ca), solar salt (Na-K), and HITEC salt. They found that all the data presented including density, viscosity, heat capacity, and thermal conductivity were dependent on temperature. The viscosity showed an Arrhenius relationship with temperature for the salt without calcium nitrate, while the Vogel-Fulcher-Tammann-Heese equation could possibly be a better fit for the viscosity of the salt with calcium nitrate. Ni et al. [14] used a molecular dynamics simulation method to study the characteristics of solar salt with the addition of 5–25 mol.% Ca^{2+}. They pointed out that the viscosities of the mixtures increased and the self-diffusion coefficients of all the ions decreased, which was due to the formation of network restricting the motion of all the ions. However, the intrinsic limitations of the thermo-physical properties of pure salts hinder their widespread applications.

Nanoparticles have been used to enhance the thermo-physical properties of pure salt [15], and the nanocomposites fabricated by salt and nanoparticles were extensively investigated both in their thermo-physical properties [16–18] and system performances [19,20]. The most important result is that the addition of nanoparticles can increase the specific heat capacities of pure salts [21]. It is also indispensable to understand and characterize the viscosities of nanocomposites, which would provide basic information for the experimental and numerical researches on how nanoparticles affect the flow of liquid salt fluid. The viscosities of the nanocomposites in a fluid state can be affected by many parameters, such as volume fraction, temperature, nanoparticle size and shape, aggregation and type of base liquid [22–24]. Jin [25] measured the viscosities of ternary nitrates using the viscometer based on the rotating cylinder method, and it was found that the addition of lithium nitrate to eutectic salt affected the viscosity slightly, while calcium nitrate would increase the viscosity of eutectic salt to some extent, e.g., the viscosity of solar salt adding calcium nitrate increased by about 53.2% at 550 K. Chen et al. [26] experimentally and theoretically studied the rheological behaviours of TiO_2 seeded ethylene glycol nanofluids, and pointed out that the concentration and structure of nanoparticles would greatly influence the viscosities of the nanofluids. Lasfargues et al. [27] measured the viscosities of solar salt and salt doped with 0.1% CuO, and it was found that the viscosities of the nanofluids increased by about 5.0~18.0% in the temperature range of 250~500 °C. Munoz-Sanchez et al. [28] measured the viscosities of solar salt seeded with alumina and silica nanoparticles at various conditions, and found out the influences of salt purity, concentration of nanoparticles, and measuring configuration of rheometer on the viscosities of solar salt. The results indicated the Newtonian behaviour of the nanofluids in spite of different rheometer configurations, and the Arrhenius model was suitable to explain the relationship between the viscosity and temperature. Jo and Banerjee [29] performed the viscosity measurements of nanofluids, which was fabricated with Li_2CO_3:K_2CO_3 (62:38) and 1 wt.%, 2 wt.% or 5 wt.% multi-walled carbon nanotubes (MWCNTs). It was found that the viscosity increased by about 93.0% with the addition of 2 wt.% MWCNT, which showed good agreement with the Krieger-Dougherty model considering the effect of nanoparticle agglomeration.

Besides the common nanoparticles, graphene has drawn researchers' attention recently and has been studied extensively [30–36]. Liu et al. [34] prepared and characterized two types of reduced graphene oxide (GO) combined with alkane, alcohol and carboxylic acid phase change materials (PCMs), and the thermal conductivity of the rGO/stearic acid composite could be increased to 3.21 (W/m·K). Kant et al. [35] pointed out that emulsifying graphene nanoparticles in PCM resulted in a relative increase of the dynamic viscosity, and significantly degraded its natural convection heat transfer performance. Furthermore, the corrosion of carbon steel with the contact of molten nitrate salt is always an important issue, and it was found that graphite could form a protective carbonate layer to improve the resistance of carbon steel [36]. Thus, adding graphene into the salt should positively affect the corrosion of container in the CSP system.

However, it can be seen that the influence of graphene on the rheological behaviour of pure salt received little attention and was seldom experimentally reported, which is an essential property affecting the flow and heat transfer characteristics of the CSP system. Moreover, the effects of the shear rates on the rheological behaviour have not been clarified and are relatively inadequate, and the data with different mass fractions of nanoparticles are still insufficient. Thus, it becomes an increasingly critical task to study the viscosities of the nanocomposites seeded with graphene and to discuss the side effects of viscosity change, which is related to the pump power of the CSP system as the nanocomposites work as HTFs. HITEC salt and solar salt were used as pure materials in the present study, aluminium oxide (Al_2O_3) nanopowder and graphene were considered as the nanoadditives. The nanocomposites were synthesized with the liquid dissolution method and were characterized with a scanning electron microscope (SEM) so as to check the combination of the nanocomposites. Then the viscosities of HITEC salt and its nanocomposites were measured using a rheometer in the temperature range of 200 °C to 450 °C, while those of solar salt were in the temperature range of 250 °C to 500 °C. The experimental results were verified with the correlations from the literature, and finally the influence of nanoparticles on flow characteristics were discussed according to the rheological behavioural results.

2. Materials and Method

2.1. Preparation of Samples

Sodium nitrite ($NaNO_2$; Alfa Aesar, UK; Purity: 98.0%), sodium nitrate ($NaNO_3$; Honeywell Fluka, UK; Purity: 99.0%) and potassium nitrate (KNO_3; Acros Organics, UK; Purity: 99.0%) were used as the base PCMs, and Al_2O_3 nanopowder (40–80 nm APS, Nanostructured & Amorphous Materials Inc., US) and graphene (the synthesis method mentioned in the previous investigation [37]) were considered as the nanoadditives. Firstly, $NaNO_2$, $NaNO_3$ and KNO_3 with mass ratios of 40:7:53 named HITEC salt were prepared with the mass balance (KERN, ABT 220-5DM), then deionized water was added into the beaker filled with the salt. The mixture was then stirred for 20 min to form the solution, which was sonicated for 1 h with an ultrasonicator at the frequency of 40 kHz to ensure good dispersion, as shown in Figure 1. Secondly, Al_2O_3 nanopowder and graphene with a mass fraction of 1% or 2% were added into the former solution without a dispersing agent, and the mixture was stirred and sonicated for 1 h with the ultrasonicator again. Finally, the solution after sonication was heated in a muffle furnace at the temperature of 200 °C to evaporate the water and melt the mixture to ensure the homogeneities of the samples. A method similar was used for the solar salt nanocomposites, except $NaNO_3$ and KNO_3 with a mass ratio of 60:40 and a heating temperature of 250 °C were used. The melting characteristics of HITEC salt and solar salt were verified with different scanning calorimeter (DSC) tests, and the DSC results of the salts seeded with nanoparticles also proved that the liquid dissolution method did not change the composition of the salts [37,38].
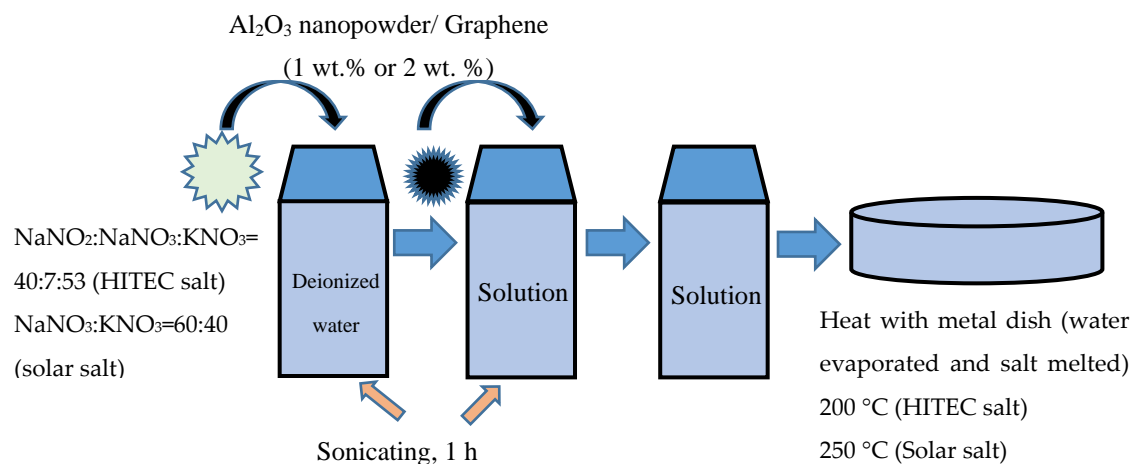
Figure 1. Synthesis of nanocomposite with liquid dissolution method. A HITEC salt/nanoparticle nanocomposite was synthesized under the heating temperature of 200 °C, while a solar salt/nanoparticle nanocomposite was heated at 250 °C.

2.2. Characterization of Nanocomposites and Nanoparticles

The morphologies of the samples were characterized by SEM (Tabletop Microscope, Model TM3030Plus, Hitachi High-Technology, Japan), while BSE (Backscattered Electrons) and EDX (Energy Dispersive X-ray Spectrometer) mode were used. In the present study, the distributions of the nanoparticle sizes were measured with a Malvern Nanosizer (Malvern Instruments Limited, Malvern, UK), which was based on dynamic light scatting (DLS) method according to the hydrodynamic diameter of nanoparticles. The method of the preparation of nanofluids was the same as that of Award et al. [39], Al_2O_3 nanopowder and graphene were dispersed in distilled water with a concentration of about 0.1%, then the nanofluids without any surfactant for stability were sonicated for about 2 h. The number of nanoparticles of each diameter were determined subsequently after the measurements. The modal distribution named intensity of nanoparticles were obtained as the measurements were repeated three times for each sample.

2.3. Measurement of Viscosity

The measurements of viscosity were conducted with an Anton Paar viscometer (Physica Modular Compact Rheometer (MCR) 502, Anton Paar, St Albans, UK), which was fitted with a convection oven and a temperature controller (TC30). The temperature controller can stabilize the sample temperature from 0 °C to 1000 °C with an accuracy of 0.1 °C. The chamber selected was a convection temperature device (CTD1000) assembly, and the measuring shaft was with parallel plate (PP35). Both PT100 sensor and heater cable were included in the measuring system. In addition, two removable connectors for air/nitrogen supply were mounted on the side surfaces of the chamber, and air hoses with the diameter of 6 mm were used to supply air or gas. An MCR 502 with PP35 is suitable for high viscous samples and samples with small particles and can conduct the measurements with high shear rate range, where temperature equilibration can be quickly obtained. However, different shear rates within the gap and sample drying effects are the disadvantages of this parallel plate system.

The parallel plate rheometer of two parallel disks was employed in the measurements, as shown in Figure 2a,b. The stainless-steel disk had a diameter of 35.0 mm and no angle, and the concentric cylinder partnered was about 40.0 mm. Once the parallel plate was fitted, the motor was warmed up for a period of about 1 h at 17,000 s^{-1} prior to any measurement been made. Then the motor adjustment and calibration were carried out to ensure the following measurements and yield reliable data. Once the motor had been stabilized, the shaft was moved into its measuring position of 1.0 mm and the experiment was started.
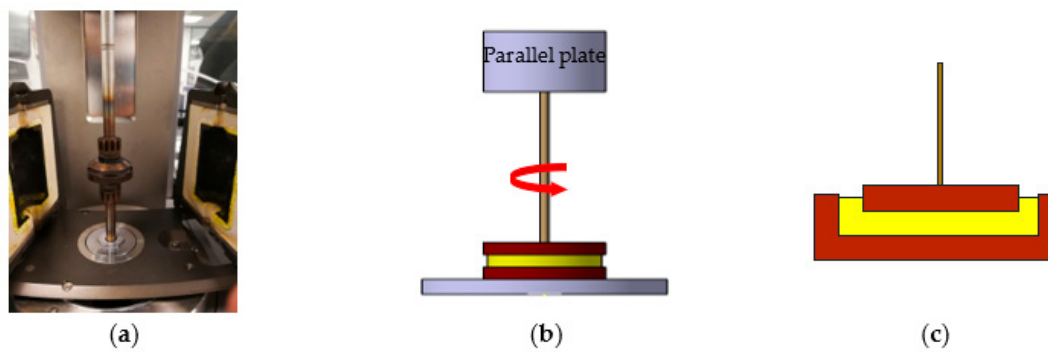
Figure 2. Rheometer used in the measurement. (**a**) MCR 502, (**b**) geometry of the rheometer, parallel plate, (**c**) schematic of loaded sample.

All experiments were conducted under a shear-rate-controlled mode. A small and similar amount (2.0 g) of sample size was placed between the parallel disks, where the controlled amount was required so as not to alter the contact area, as shown in Figure 2c. The excess sample was removed at a trim position when the shaft was moved into its measuring position. Furthermore, it was indispensable to ensure the cleanliness of both geometries before and after each measurement. The measurements for the samples were conducted under various shear rates between 1 s^{-1} and 250 s^{-1}, and the setting loop was 30 points with natural logarithm decrease in shear rate. The measuring temperatures were 200 °C, 250 °C, 300 °C, 350 °C, 400 °C and 450 °C for HITEC salt and its nanocomposites, 250 °C, 300 °C, 350 °C, 400 °C, 450 °C and 500 °C for solar salt and its nanocomposites, which are listed in Table 1.

Table 1. Viscosity measurements of salts and nanocomposites in the present study.

Material Type	Nanoparticle (Al$_2$O$_3$ Nanopowder, Graphene)			Temperature (°C)
HITEC salt	0%	1 wt.%	2 wt.%	200, 250, 300, 350, 400, 450
solar salt	0%	1 wt.%	2 wt.%	250, 300, 350, 400, 450, 500

## 3. Results and Discussion

3.1. Characterization of Nanocomposites

Figure 3 shows the SEM pictures of the nanocomposites. It can be seen from Figure 3a,b that Al$_2$O$_3$ nanopowder can generate structural interaction with salt molecules, as it is difficult to distinguish the nanoparticle from salt. The rugged surface is caused by the shrinkage of salt during freezing, due to the density difference of salt in solid and liquid states. The salt is generally compatible with graphene, while several graphene are agglomerated on the surface of the samples, as shown in Figure 3c,d. The good combination and dispersion are of great importance as only a small amount was used in the measurements.
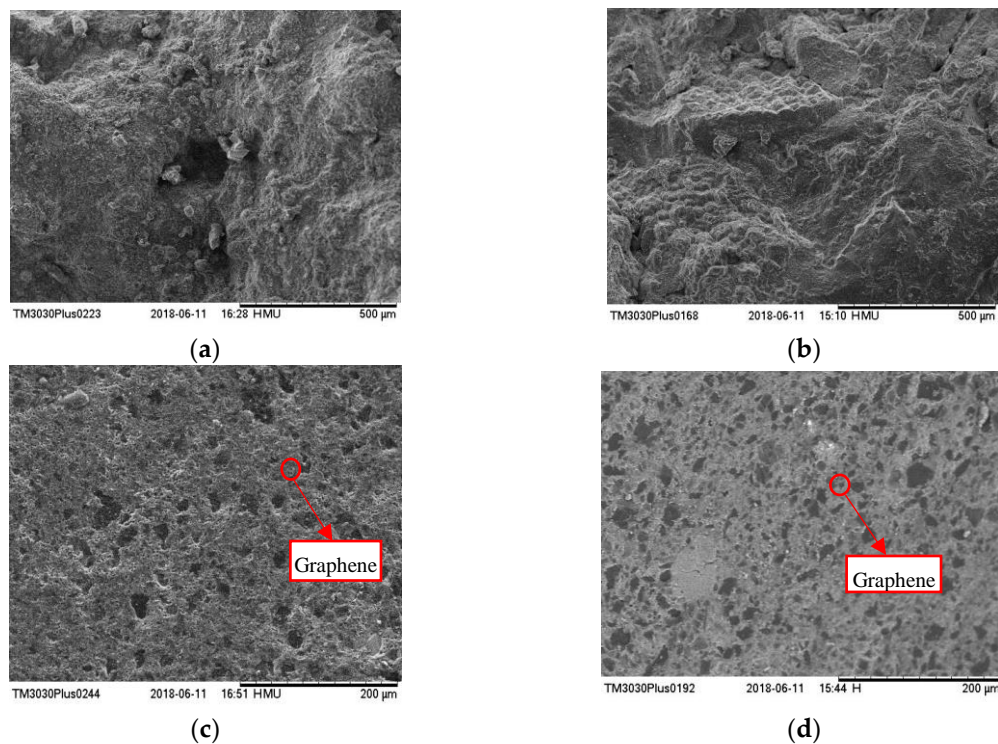
Figure 3. SEM images of nanocomposites. (**a**) HITEC salt/2 wt.% Al_2O_3 nanopowder, (**b**) solar salt/2 wt.% Al_2O_3 nanopowder, (**c**) HITEC salt/2 wt.% graphene, (**d**) solar salt/2 wt.% graphene.

3.2. Rheological Behaviour of Pure Salt

In the present study, the rheological behaviours of HITEC salt and solar salt at both high and low shear rates were measured. The viscosities and shear stresses against the shear rates of 25 s^{-1} to 250 s^{-1} are shown in Figure 4a,b. It can be seen that the viscosities are almost constant with various shear rates, while the viscosities slightly increase when the shear rate exceeds 100 s^{-1} due to the uncertainty of the measurements caused by the residual force. The shear stresses and shear rates are almost linear dependent, which proves the Newtonian behaviour of HITEC salt. Figure 4c,d show the viscosities and shear stresses against the shear rates below 25 s^{-1}. Large fluctuation can be found both for the viscosities and shear stresses, and the Newtonian behaviour is not obvious in the period due to low torque resolution, where the same phenomenon can be seen in the literature [27,28]. Thus, the values below 25 s^{-1} were discarded, and only the shear rates between 25 s^{-1} and 250 s^{-1} were taken into account in the following discussion.
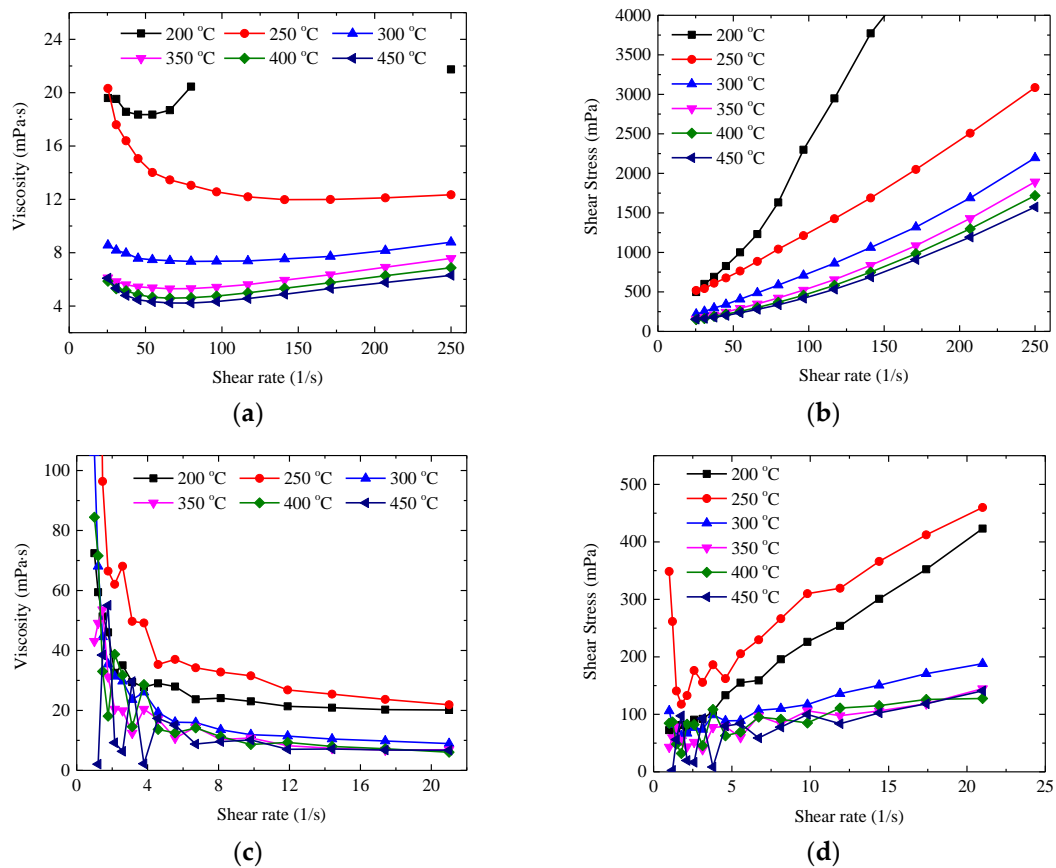
Figure 4. Viscosities and shear stresses against different shear rates for HITEC salt. (**a**) viscosity (25 s^{-1} to 100 s^{-1}), (**b**) shear stress (25 s^{-1} to 100 s^{-1}), (**c**) viscosity (1 s^{-1} to 25 s^{-1}), (**d**) shear stress (1 s^{-1} to 25 s^{-1}).

The viscosities and shear stresses for solar salt against the shear rates of 25 s^{-1} to 250 s^{-1} are shown in Figure 5a,b. Similarly, the viscosities are almost constant with various shear rates, while the viscosities slightly increase when the shear rate exceeds 100 s^{-1} due to the same reason of the residual force. The shear stresses and shear rates are almost linear dependent, which also proves the Newtonian behaviour of solar salt. Figure 5c,d show the viscosities and shear stresses against the shear rates below 25 s^{-1}. The fluctuation is better than those of HITEC salt but still exist for various viscosities and shear stresses, and the Newtonian behaviour is not completely provable. The whole characteristics are the same as the nanofluids studied by Munoz-Sanchez et al. [28], where the viscosities were nearly constant at shear rates of $100\sim250 \text{ s}^{-1}$ both with coaxial cylinder rheometer and parallel plate rheometer. Thus, being the same as HITEC salt, only the shear rates between 25 s^{-1} and 250 s^{-1} were taken into account in the following discussion. The reduction of the fluctuation can be attributed to the binary melting characteristics of solar salt, which will be described subsequently.
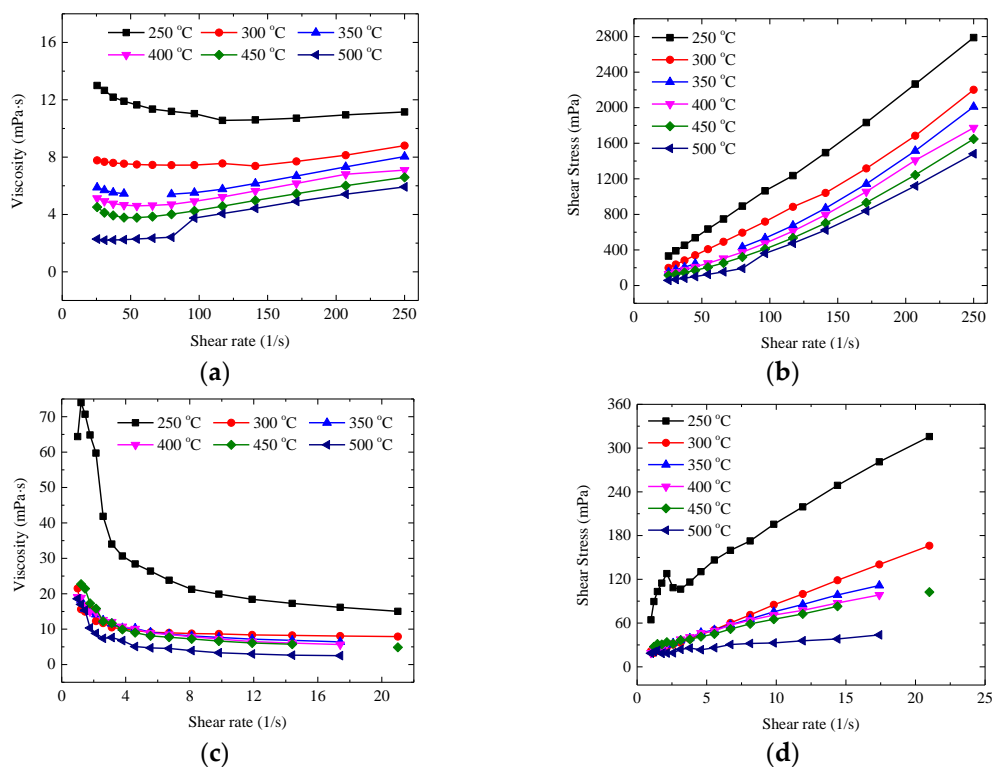
Figure 5. Viscosities and shear stresses against different shear rates for solar salt. (**a**) viscosity (25 s^{-1} to 100 s^{-1}), (**b**) shear stress (25 s^{-1} to 100 s^{-1}), (**c**) viscosity (1 s^{-1} to 25 s^{-1}), (**d**) shear stress (1 s^{-1} to 25 s^{-1}).

Comparison with Literature Correlations

Table 2 lists all the correlations obtained from the literature, which are for the viscosities of HITEC salt and solar salt varying with temperatures. The present results of the viscosities were compared with the correlations in Table 2, as shown in Figure 6a,b. The curves in Figure 6 based on the correlations from the literature [25,27,40–48] were obtained from seven temperature points, including the minimum and maximum temperatures of the temperature range in Table 2, five temperature points among the range. It can be seen that the viscosities in the present study are larger than those in the literature to some extent, especially under the low temperature. The discrepancy can be attributed to the following reason. On one hand, the salts used in the present study might slightly differ from those in the literature, such as purity and amount. On the other hand, PP35 as flat parallel plate used in the measurements caused residual force during the rotation. As a result, it increased the uncertainty of the measurements and induced the deviation. The same discrepancy was reported in the experimental investigations of Munoz-Sanchez et al. [28], and their results were also much higher than those from the literature, due to the amount of solid particles in the salt.

Table 2. Viscosities of salts varying with temperatures by fitting the following literature correlations [25,27,40–48].

Material Type	Fitting Curves	Measure Methods	Temperature Range	Reference
HITEC salt	$\mu = T^{-2.104} \times 10^{5.7374}$	Rotating method	150~500 °C	[40]
	$\mu = 1.149 \cdot \exp\left[-810.896/(T+273) + 7.806 \times 10^5/(T+273)^2\right]$	Rotational coaxial cylinder method	147~422 °C	[25]
	$\mu = 67.57 \times 10^{-3} \cdot \exp[2247.11/(T+273)]$	Ostwald rheometer	182~507 °C	[41]
	$\mu = 0.5631 \cdot \exp\left[-146.9794(T+273)^{-1} + 57.4265 \times 10^4(T+273)^{-2}\right]$	Oscillating rheometer	184~482 °C	[42]
	$\mu = 0.75484 \cdot \exp[6418/R(T+273)]$	Oscillation cup method	250~450 °C	[43]
	$\mu = 1000 \cdot \exp(-4.343 - 2.0143 \ln T - 5.011)$	Oscillation cup method	247~500 °C	[44]
solar salt	$\mu = 79786 \cdot (T+273)^{-1.773}$	Rotational coaxial cylinder method	250~550 °C	[27]
	$\mu = 5.103 \cdot \exp\left[-2.575 \times 10^3/(T+273) + 1.305 \times 10^6/(T+273)^2\right]$	Rotational coaxial cylinder method (commercial)	243~447 °C	[25]
	$\mu = 2.551 \cdot \exp\left[-1.65 \times 10^3/(T+273) + 1.022 \times 10^6/(T+273)^2\right]$	Rotational coaxial cylinder method	233~440 °C	[25]
	$\mu = \exp[2210/(T+273) - 2.48]$	Rheometric ARES rheometer	222~547 °C	[45]
	$\mu = 22.174 - 0.12 \cdot T + 2.281 \times 10^{-4} \cdot T^2 - 1.474 \times 10^{-7} \cdot T^3$	Oscillation cup method	275~600 °C	[46,47]
	$\mu = 0.4384 \cdot \exp\left[-9.2163/(T+273) + 6.52 \times 10^5/(T+273)^2\right]$	Oscillating sphere method	250~450 °C	[48]
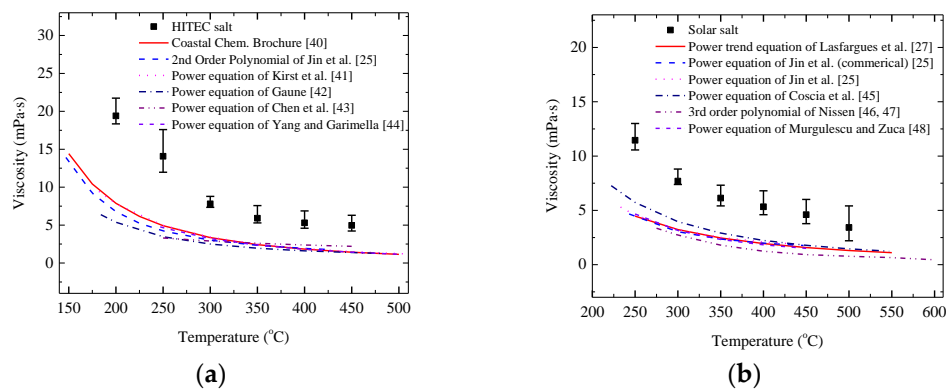
Figure 6. Comparison of present experimental results of viscosities with experimental data reported in the literature [25,27,40–48]. (**a**) HITEC salt; (**b**) solar salt.

*3.3. Rheological Behaviour of Nanocomposite*

3.3.1. Size of Nanoparticles

The sizes of Al_2O_3 nanopowder and graphene were measured with the DLS method in the present study. Figure 7 shows the size distributions of the two nanofluids. The tests were repeated, and the average sizes of Al_2O_3 nanopowder and graphene were about 222.6 nm and 356.4 nm, respectively. It can be seen that the size of Al_2O_3 nanopowder was significantly larger than the parameter from the manufacturer, which was about 40~80 nm. The possible reason for the larger nanoparticle size is that the nanoparticles would suffer from agglomeration as no surfactant was used to stabilize the nanofluid.
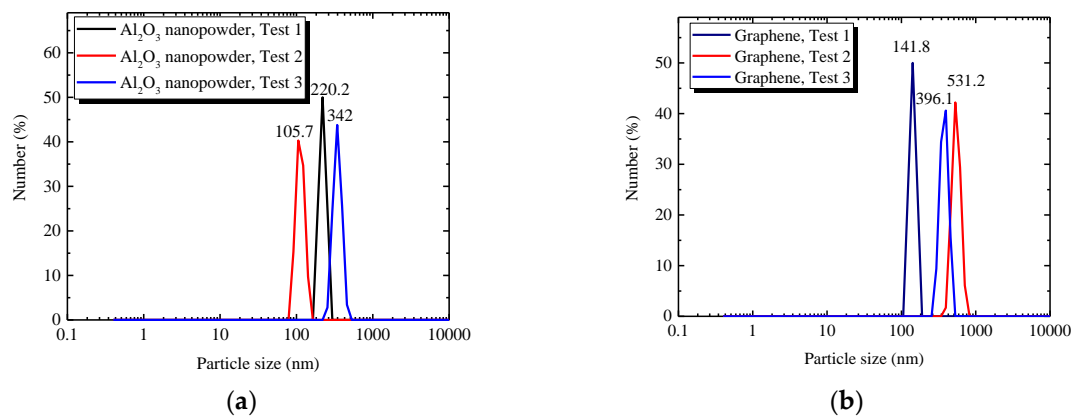
Figure 7. Sizes for different nanoparticles with DLS device. (**a**) Al_2O_3 nanopowder nanofluid; (**b**) graphene nanofluid.

3.3.2. Viscosity of Nanocomposites

Figure 8 shows the viscosities of the HITEC salt nanocomposites against different shear rates, where both Al_2O_3 nanopowder and graphene were included. The viscosities of the salt seeded with Al_2O_3 nanopowder were generally constant at different shear rates in the range between $25\,s^{-1}$ and $250\,s^{-1}$, and the viscosities decreased with the increase of temperatures regularly, as shown in Figure 8a. However, the viscosities slightly increased with the increase of shear rates when the shear rates were larger than $100\,s^{-1}$. The variation is attributed to the following reasons. On one hand, the shear rates might affect the interactions among nanoparticles, inducing the agglomeration. On the other hand, the uncertainty of the device may cause the deviation of the results, as the concentration of Al_2O_3 nanopowder larger than those in the literature [27] affects the flow of liquid salt significantly. Furthermore, the viscosities of the nanocomposites with the addition of 2 wt.% Al_2O_3 nanopowder were generally larger than those with 1 wt.% Al_2O_3 nanopowder no matter what the shear rate was, especially at high temperature.
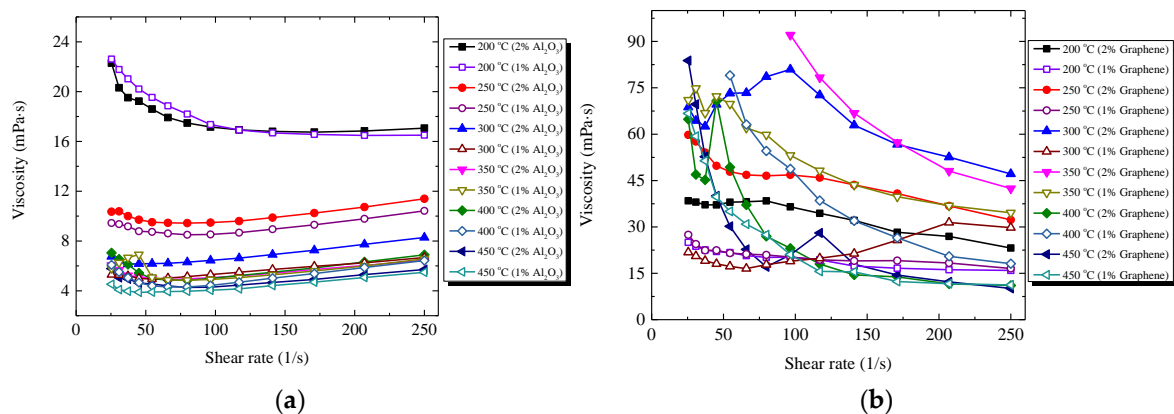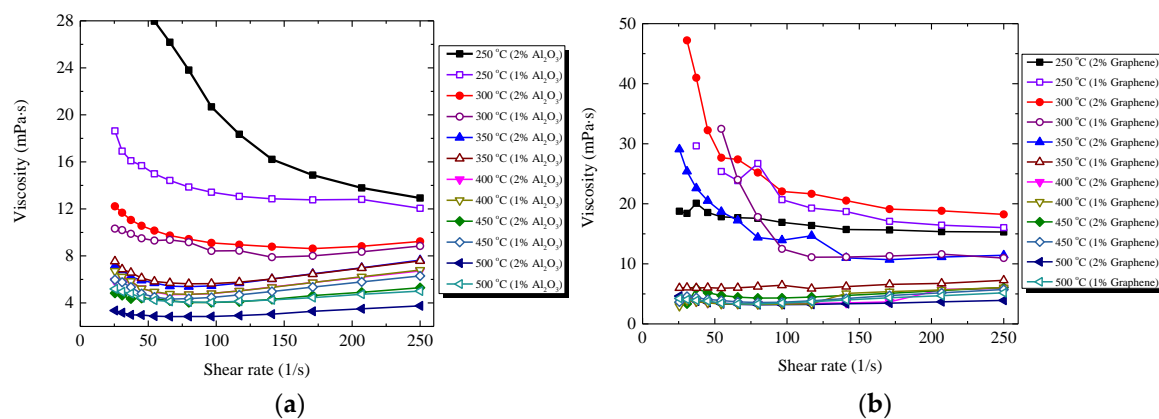

Figure 8. Viscosities of nanocomposites against different shear rates. (**a**) HITEC salt seeded with Al_2O_3 nanopowder, (**b**) HITEC salt seeded with graphene. The addition of Al_2O_3 nanopowder and graphene is with mass weight percentage.

The rheological behaviour of HITEC salt seeded with graphene was different from the nanocomposite seeded with Al_2O_3 nanopowder to some extent, as shown in Figure 8b. The viscosities slightly decreased with the increase of shear rates, and the fluctuation was obvious especially at the temperatures of 400 °C and 450 °C. The possible reason is that graphene with a slice structure might be separated at higher shear rate, which decreases the viscosity accordingly. The viscosities decrease with the increase of the temperature regularly when the temperature is higher than 350 °C, but it is

irregular when the temperature is under 350 °C, i.e., the largest viscosity of HITEC salt seeded with graphene happens at 300~350 °C with the addition of 2 wt.% graphene. The phenomenon can be attributed to the following reasons: On one hand, the measurement includes great uncertainty at low temperature as slice graphene greatly affects the flow of liquid salt. On the other hand, the addition of graphene into HITEC salt slightly induces the non-Newtonian behaviours of the nanocomposites, and the ternary melting characteristics of HITEC salt might be slightly changed with graphene. Similarly, the viscosities of the nanocomposites with the addition of 2 wt.% graphene are generally larger than those with 1 wt.% graphene.

Figure 9 shows the viscosities of the solar salt nanocomposites against different shear rates, where both Al_2O_3 nanopowder and graphene are also included. Comparing Figure 8a with Figure 9a, it is found that the viscosities of solar salt seeded with Al_2O_3 nanopowder were generally constant at different shear rates similarly, and the viscosities slightly increased with the increase of shear rates when the shear rates were larger than 100 s^{-1}. The possible reasons should be similar to those of HITEC salt, including the agglomeration of nanoparticles and the uncertainty of the measurement. Figure 9b shows that the rheological behaviours of solar salt seeded with graphene were different from those of HITEC salt seeded with graphene shown in Figure 8b. The plateau region in the curve represents that the viscosities of solar salt seeded with graphene were generally constant at different shear rates, which indicates that the binary melting characteristics of solar salt can be kept well. No matter which nanoparticle it is, the viscosities of the nanocomposites decreased with the increase of temperatures regularly.

Figure 9. Viscosities of nanocomposites against different shear rates. (**a**) solar salt seeded with Al_2O_3 nanopowder, (**b**) solar salt seeded with graphene. The addition of Al_2O_3 nanopowder and graphene is with mass weight percentage.

Figure 10 and Table 3 present the comparisons of the viscosities of the salts and nanocomposites, both for HITEC salt and solar salt. Because the formation of a vortex structure near the surface of the nanoparticle promotes a rotational movement [26], the addition of nanoparticles into the salts lead to an increase in viscosity. The increase is noticeable at low temperature below 400 °C, but that is unobvious at high temperature of 400~500 °C for solar salt. The possible reason is that the Brownian motion of nanoparticles may be enhanced at high temperature.
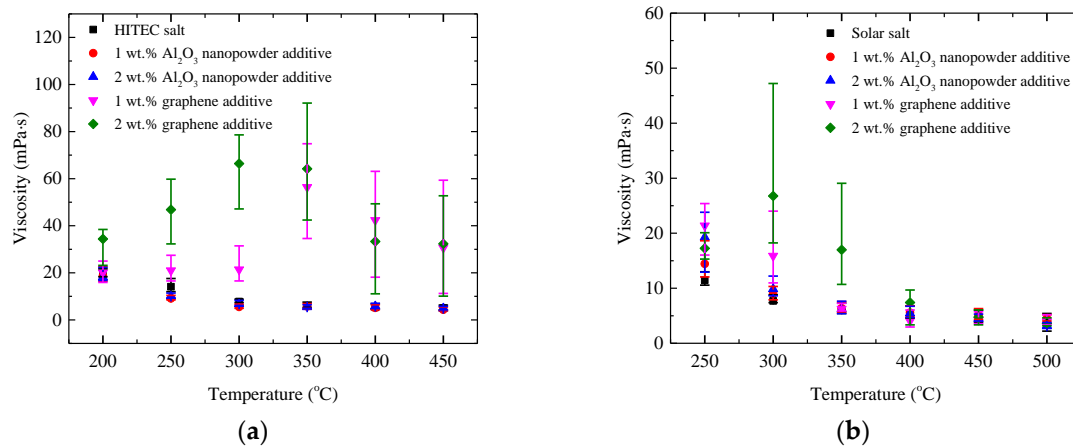
Figure 10. Viscosities of salt and nanocomposites against different temperatures. (**a**) HITEC salt and its nanocomposites, (**b**) solar salt and its nanocomposites.

Table 3. Average dynamic viscosities of salts and nanocomposites in the present study.

Material Type	Viscosities (mPa·s)						
	200 °C	250 °C	300 °C	350 °C	400 °C	450 °C	500 °C
HITEC salt	19.41	14.08	7.80	5.90	5.30	4.97	-
HITEC salt/1 wt.% Al$_2$O$_3$ nanopowder	18.67	9.09	5.48	5.68	5.08	4.32	-
HITEC salt/2 wt.% Al$_2$O$_3$ nanopowder	18.22	10.01	6.73	5.44	5.74	4.84	-
HITEC salt/1 wt.% Graphene	20.12	21.00	21.39	56.37	42.35	30.62	-
HITEC salt/2 wt.% Graphene	34.36	46.82	66.41	64.18	33.32	32.30	-
solar salt	-	11.46	7.69	6.13	5.33	4.60	3.42
solar salt/1 wt.% Al$_2$O$_3$ nanopowder	-	14.43	9.05	6.36	5.57	5.13	4.50
solar salt/2 wt.% Al$_2$O$_3$ nanopowder	-	19.26	9.87	6.22	5.46	4.47	3.11
solar salt/1 wt.% Graphene	-	21.38	15.88	6.26	4.06	4.24	3.96
solar salt/2 wt.% Graphene	-	17.25	26.76	16.98	7.41	4.75	3.60

It can be seen from Figure 10 and Table 3 that the addition of Al$_2$O$_3$ nanopowder leads to slight changes in the viscosities of pure salt, e.g., the viscosities can be changed with the range of −35.4~8.1% for the HITEC salt nanocomposites and with the range of −9.2~68.1% for the solar salt nanocomposites. The decrease of viscosities was mainly due to the uncertainty of the measurement. Similarly, the addition of 0.1 wt.% copper oxide into solar salt led to an increase of 4.7~18.3% in viscosity with the temperature range of 250~450 °C, as shown in the literature [27]. While in the research of Munoz-Sanchez et al. [28], the refined grade solar salt (RSS) nanofluid containing 1.5 wt.% alumina nanoparticles had a variation of −14.71~0.63% in viscosity with the temperature range of 300~400 °C. On the contrary, the RSS nanofluid containing 1.5 wt.% Silica nanoparticles had an increase of 3.49~21.75% in viscosity with the temperature range of 300~400 °C.

In a preliminary DSC tests, no obvious change of heat flow was found from the melting phase change temperature to 500 °C, indicating that there was no chemical reaction between graphene and salt. But the addition of graphene leads to a remarkable increase of viscosities, e.g., the addition of 2 wt.% graphene into HITEC salt causes an increase of 77.0%, 232.5%, 751.4%, 987.3%, 528.2% and 550.2% for 200 °C, 250 °C, 300 °C, 350 °C, 400 °C and 450 °C, respectively, while the addition of 2 wt.% graphene into solar salt causes an increase of 50.5%, 247.9%, 176.8%, 39.1%, 3.2% and 5.1% for 250 °C, 300 °C, 350 °C, 400 °C, 450 °C and 500 °C, respectively. The difference can be attributed to different sizes and shapes of the nanoparticles. It was found that the average size of graphene was larger than that of Al$_2$O$_3$ nanopowder, as mentioned previously in Section 3.3.1. The larger size of the nanoparticle would restrict the flow of liquid salt and increase the viscosity correspondingly. Besides the difference of the nanoparticle size, the different structural characteristics between graphene and Al$_2$O$_3$ nanopowder shown in the literature [37,38] also affect the viscosity of the nanocomposites. In

accordance with Figures 8b and 9b, the large increment in viscosity indicates that HITEC salt seeded with graphene shows non-Newtonian behaviour slightly.

In all, the viscosity of the salt worked as the HTF in a CSP system is related to the pump power in the plant, the addition of the nanoparticles induce large viscosities and are likely to raise the cost of the pump power. The suitable ratio of addition of nanoparticles into the PCMs should be considered in the real applications although nanocomposites are with good thermo-physical properties.

4. Conclusions

In the present study, HITEC salt and solar salt were used as pure materials, and the nanocomposites were synthesized with the salt and 1 wt. % or 2 wt.% Al_2O_3 nanopowder and graphene by liquid dissolution method. The evolutions of the viscosities of HITEC salt and its nanocomposites in the temperature ranges from 200 °C to 450 °C, solar salt and its nanocomposites in the temperature ranges from 250 °C to 500 °C were measured with the rheometer and analysed subsequently. The following conclusions can be drawn:

(1) The viscosities of pure HITEC salt and solar salt regularly decrease with the increase of temperatures and demonstrate the Newtonian behaviour at different temperature ranges. The present results show reasonable agreement with the calculation results from the literature correlations to some extent, while the deviation was mainly caused by parallel plate and purity of salt.

(2) Both Al_2O_3 nanopowder and graphene are compatible with molten salt and can generate structural interaction with salt molecules. Agglomeration of graphene happens on the surface of the salts seeded with graphene. A better method to synthetize the nanocomposites seeded with graphene should be investigated in the future.

(3) The viscosities of all the nanocomposites show temperature dependence. The addition of Al_2O_3 nanopowder into the salt has relatively little effect on the viscosity of the salt, e.g., the viscosities vary with the range of $-35.4\sim8.1\%$ for the HITEC salt nanocomposites and with the range of $-9.2\sim68.1\%$ for the solar salt nanocomposites. Whereas graphene leads to a remarkable increase in viscosities, especially at low temperature below 400 °C, which should be due to the larger size and different structural characteristics of graphene.

(4) Experimental results reveal that the addition of graphene into HITEC salt induces the non-Newtonian behaviours of the nanocomposites, and the ternary melting characteristics of HITEC salt might be changed with graphene. While solar salt seeded with graphene shows Newtonian behaviour at different shear rates and temperatures, indicating that the binary melting characteristics of solar salt can be kept well.

Because graphene can provide a positive effect on the issue of corrosion in addition to the improvement of thermo-physical properties, it is important to investigate the system performance of the salts seeded with graphene. A systematic test rig to study the flow and heat transfer characteristics of salts seeded with graphene working as HTFs is essential, so as to promote the utilization of the nanocomposites in the real applications.

Nomenclature

T	temperature, °C
R	ideal gas constant, J/(K·mol)
Greek letters	
μ	dynamic viscosity, mPa·s
Acronyms	
BSE	backscattered electrons
CSP	concentrated solar power
CTD	convection temperature device
DLS	dynamic light scatting
EDX	energy dispersive X-ray spectrometer
HTF	heat transfer fluid
MWCNT	multi-walled carbon nanotubes
PP	parallel plate
SEM	scanning electron microscope

References

1. Wang, S.; Brian Tarroja, B.; Schell, L.S.; Shaffer, B.; Samuelsen, S. Prioritizing among the end uses of excess renewable energy for cost-effective greenhouse gas emission reductions. *Appl. Energy* **2019**, *235*, 284–298. [CrossRef]
2. Romeroa, M.; Steinfeld, A. Concentrating solar thermal power and thermochemical fuels. *Energy Environ. Sci.* **2012**, *5*, 9234–9245. [CrossRef]
3. Maldonado, J.M.; Fullana-Puig, M.; Martín, M.; Solé, A.; Fernández, A.G.; Gracia, A.; Cabeza, L.F. Phase change material selection for thermal energy storage at high temperature range between 210 °C and 270 °C. *Energies* **2018**, *11*, 861. [CrossRef]
4. Fernandez-García, A.; Rojas, E.; Perez, M.; Silva, R.; Hernandez-Escobedo, Q.; Manzano-Agugliaro, F. A parabolic-trough collector for cleaner industrial process heat. *J. Clean. Prod.* **2015**, *89*, 272–985. [CrossRef]
5. Fernandez-García, A.; Juaidi, A.; Sutter, F.; Martinez-Arcos, L.; Manzano-Agugliaro, F. Solar reflector materials degradation due to the sand deposited on the backside protective paints. *Energies* **2018**, *11*, 808. [CrossRef]
6. Fernandez-García, A.; Valenzuela, L.; Zarza, E.; Rojas, E.; Perez, M.; Hernandez-Escobedo, Q.; Manzano-Agugliaro, F. SMALL-SIZED parabolic-trough solar collectors: Development of a test loop and evaluation of testing conditions. *Energy* **2018**, *152*, 401–415. [CrossRef]
7. Mostafavi Tehrani, S.S.; Taylor, R.A.; Nithyanandam, K.; Shafiei Ghazani, A. Annual comparative performance and cost analysis of high temperature, sensible thermal energy storage systems integrated with a concentrated solar power plant. *Sol. Energy* **2017**, *153*, 153–172. [CrossRef]
8. Xu, B.; Li, P.W.; Chan, C. Application of phase change materials for thermal energy storage in concentrated solar thermal power plants: A review to recent developments. *Appl. Energy* **2015**, *160*, 286–307. [CrossRef]
9. Xiao, X.; Zhang, P.; Li, M. Thermal characterization of nitrates and nitrates/expanded graphite mixture phase change materials for solar energy storage. *Energy Convers. Manag.* **2013**, *73*, 86–94. [CrossRef]
10. Zhang, P.; Xiao, X.; Meng, Z.N.; Li, M. Heat transfer characteristics of a molten-salt thermal energy storage unit with and without heat transfer enhancement. *Appl. Energy* **2015**, *137*, 758–772. [CrossRef]
11. Bonka, A.; Sau, S.; Uranga, N.; Hernaiz, M.; Bauer, T. Advanced heat transfer fluids for direct molten salt line-focusing CSP plants. *Prog. Energy Combust.* **2018**, *67*, 69–87. [CrossRef]
12. Xiao, X.; Zhang, P.; Li, M. Experimental and numerical study of heat transfer performance of nitrates/expanded graphite composite PCM for solar energy storage. *Energy Convers. Manag.* **2015**, *105*, 272–284. [CrossRef]
13. Siegel, N.P.; Bradshaw, R.W.; Cordaro, J.B.; Kruizenga, A.M. Thermophysical property measurement of nitrate salt heat transfer fluids. In Proceedings of the ASME 2011 5th International Conference on Energy Sustainability, Washington, DC, USA, 7–10 August 2011.
14. Ni, H.O.; Wu, J.; Sun, Z.; Lu, G.M.; Yu, J.G. Insight into the viscosity enhancement ability of Ca(NO$_3$)$_2$ on the binary molten nitrate salt: A molecular dynamics simulation study. *Chem. Eng. J.* **2018**. [CrossRef]

15. Wu, Y.T.; Li, Y.; Ren, N.; Ma, C.F. Improving the thermal properties of NaNO₃-KNO₃ for concentrating solar power by adding additives. *Sol. Energy Mater. Sol. Cells* **2018**, *176*, 357–373.

16. Owolabi, A.L.; Al-Kayiem, H.H.; Baheta, A.T. Nanoadditives induced enhancement of the thermal properties of paraffin-based nanocomposites for thermal energy storage. *Sol. Energy* **2016**, *135*, 644–653. [CrossRef]

17. Myers, P.D., Jr.; Alam, T.E.; Kamal, R.; Goswami, D.Y.; Stefanakos, E. Nitrate salts doped with CuO nanoparticles for thermal energy storage with improved heat transfer. *Appl. Energy* **2016**, *165*, 225–233. [CrossRef]

18. Arthur, O.; Karim, M.A. An investigation into the thermophysical and rheological properties of nanofluids for solar thermal applications. *Renew. Sustain. Energy Rev.* **2016**, *55*, 739–755. [CrossRef]

19. Al-Jethelah, M.; Tasnim, S.H.; Mahmud, S.; Dutta, A. Nano-PCM filled energy storage system for solar-thermal applications. *Renew. Energy* **2018**, *126*, 137–155. [CrossRef]

20. Elbahjaoui, R.; QarniaCad, H.E. Thermal analysis of nanoparticle-enhanced phase change material solidification in a rectangular latent heat storage unit including natural convection. *Energy Build.* **2017**, *153*, 1–17. [CrossRef]

21. Shin, D.Y.; Banerjee, D. Specific heat of nanofluids synthesized by dispersing alumina nanoparticles in alkali salt eutectic. *Int. J. Heat Mass Transfer* **2014**, *74*, 210–214. [CrossRef]

22. Huminic, A.; Huminic, G.; Fleaca, C.; Dumitrache, F.; Morjan, I. Thermal conductivity, viscosity and surface tension of nanofluids based on FeC nanoparticles. *Powder Technol.* **2015**, *284*, 78–84. [CrossRef]

23. Bashirnezhad, K.; Bazri, S.; Safaei, M.R.; Goodarzi, M.; Dahari, M.; Mahian, O.; Dalkiliça, A.S.; Wongwises, S. Viscosity of nanofluids: A review of recent experimental studies. *Int. Commun. Heat Mass Transf.* **2016**, *73*, 114–123. [CrossRef]

24. Prasher, R.; Song, D.; Wang, J.; Phelan, P. Measurements of nanofluid viscosity and its implications for thermal applications. *Appl. Phys. Lett.* **2006**, *89*, 133108. [CrossRef]

25. Jin, Y.; Cheng, J.H.; An, X.H.; Su, T.; Zhang, P.; Li, Z. Accurate viscosity measurement of nitrates/nitrites salts for concentrated solar power. *Sol. Energy* **2016**, *137*, 385–392. [CrossRef]

26. Chen, H.S.; Ding, Y.L.; Tan, C.Q. Rheological behaviour of nanofluids. *New J. Phys* **2007**, *9*, 367. [CrossRef]

27. Lasfargues, M.; Cao, H.; Geng, Q.; Ding, Y.L. Rheological analysis of binary eutectic mixture of sodium and potassium nitrate and the effect of low concentration CuO nanoparticle addition to its viscosity. *Materials* **2015**, *8*, 5194–5204. [CrossRef] [PubMed]

28. Munoz-Sancheza, B.; Nieto-Maestrea, J.; Veca, E.; Liberatore, R.; Sau, S.; Navarro, H.; Ding, Y.L.; Navarrete, N.; Enrique, J.J.; Ángel, G.; et al. Rheology of solar-salt based nanofluids for concentrated solar power. Influence of the salt purity, nanoparticle concentration, temperature and rheometer geometry. *Sol. Energy Mater. Sol. Cells* **2018**, *176*, 357–373. [CrossRef]

29. Jo, B.; Banerjee, D. Viscosity measurements of multi-walled carbon nanotubes-based high temperature nanofluids. *Mater. Lett.* **2014**, *122*, 212–215. [CrossRef]

30. Kumar, R.; Joanni, E.; Singh, R.K.; Singh, D.P.; Moshkalev, S.A. Recent advances in the synthesis and modification of carbon-based 2D materials for application in energy conversion and storage. *Prog. Energy Combust.* **2018**, *67*, 115–157. [CrossRef]

31. Choi, H.J.; Jung, S.M.; Seo, J.M.; Chang, D.W.; Dai, L.M.; Baek, J.B. Graphene for energy conversion and storage in fuel cells and supercapacitors. *Nano Energy* **2012**, *1*, 534–551. [CrossRef]

32. Chen, D.Z.; Qin, S.Y.; Tsui, G.C.P.; Tang, C.Y.; Ouyang, X.; Liu, J.H.; Tang, J.N.; Zuo, J.D. Fabrication, morphology and thermal properties of octadecylamine-grafted graphene oxide-modified phase-change microcapsules for thermal energy storage. *Compos. Part B* **2019**, *157*, 239–247. [CrossRef]

33. Kholmanov, I.; Kim, J.Y.; Ou, E.; Ruoff, R.S.; Shi, L. Continuous carbon nanotube-ultrathin graphite hybrid foams for increased thermal conductivity and suppressed subcooling in composite phase change materials. *ACS Nano* **2015**, *9*, 11699–11707. [CrossRef] [PubMed]

34. Liu, L.; Zheng, K.; Yan, Y.; Cai, Z.H.; Lin, S.X.; Hu, X.B. Graphene aerogels enhanced phase change materials prepared by one-pot method with high thermal conductivity and large latent energy storage. *Sol. Energy Mater. Sol. Cells* **2018**, *185*, 487–493. [CrossRef]

35. Kant, K.; Shukla, A.; Sharma, A.; Biwole, P.H. Heat transfer study of phase change materials with graphene nanoparticle for thermal energy storage. *Sol. Energy* **2017**, *146*, 453–463. [CrossRef]

36. Grosu, Y.; Nithiyanantham, U.; Zaki, A.; Faik, A. A simple method for the inhibition of the corrosion of carbon steel by molten nitrate salt for thermal storage in concentrating solar power applications. *Mater. Degrad.* **2018**, *34*, 1–8. [CrossRef]

37. Xiao, X.; Wen, D.S. Preparation and characterization of salt/nickel foam composite seeded with graphene. In Proceedings of the 6th International Conference on Cryogenics and Refrigeration, Shanghai, China, 12–14 April 2018.

38. Xiao, X.; Wen, D.S. Investigation on thermo-physical properties of molten salt enhanced with nanoparticle and copper foam. *IEEE Xplore Digital Library* **2018**. [CrossRef]

39. Award, A.; Navarro, H.; Ding, Y.L.; Wen, D.S. Thermal-physical properties of nanoparticle-seeded nitrate molten salts. *Renew. Energy* **2018**, *120*, 275–588.

40. HITEC Heat Transfer Salt. Costal Chemical Co., L.L.C., Brenntag Company. Available online: http://www.coastalchem.com (accessed on 18 December 2018).

41. Kirst, W.E.; Nagle, W.M.; Castner, J.B. A new heat transfer medium for high temperatures. *Trans. Am. Inst. Chem. Eng.* **1940**, *36*, 371–394.

42. Gaune, P.G. Viscosity of potassium nitrate-sodium nitrite-sodium nitrate mixtures. *J. Chem. Eng. Data* **1982**, *27*, 151–153. [CrossRef]

43. Chen, Y.C.; Wu, Y.T.; Ren, N.; Ma, C.F. Experimental study of viscosity characteristics of high-temperature heat transfer molten salts. *Sci. China Technol. Sci.* **2011**, *54*, 3022–3026. [CrossRef]

44. Yang, Z.; Garimella, S.V. Thermal analysis of solar thermal energy storage in a molten-salt thermocline. *Sol. Energy* **2010**, *84*, 974–985. [CrossRef]

45. Coscia, K.; Neti, S.; Oztekin, A.; Nelle, S.; Mohapatra, S.; Elliott, T. The thermophysical properties of the $NaNO_3$-KNO_3, $LiNO_3$-$NaNO_3$, and $LiNO_3$-KNO_3 systems. In Proceedings of the ASME International Mechanical Engineering Congress and Exposition, Denver, CO, USA, 11–17 November 2012.

46. Nissen, D.A. Thermophysical properties of the equimolar mixture $NaNO_3$-KNO_3 from 300 to 600 °C. *J. Chem. Eng. Data* **1982**, *27*, 269–273. [CrossRef]

47. Mar, R.W.; Bradshaw, R.W.; Carling, R.W.; Goods, S.H.; Nagelberg, A.S.; Nissen, D.A. *Progress Report: Molten Nitrate Salt Technology Development*; SAND82-8220; Sandia National Labs: Livermore, CA, USA, 1982.

48. Murgulescu, I.G.; Zuca, S. Viscosity of binary mixtures of molten nitrates as a function of ionic radius-II. *Electrochim. Acta* **1969**, *14*, 519–526. [CrossRef]